Influence of surface load variations on eruption likelihood: application to two Icelandic subglacial volcanoes, Grímsvötn and Katla

F. Albino, V. Pinel, F. Sigmundsson

Geophysical Journal International

Geophys. J. Int. (2010) **181,** 1510–1524 doi: 10.1111/j.1365-246X.2010.04603.x

Influence of surface load variations on eruption likelihood: application to two Icelandic subglacial volcanoes, Grímsvötn and Katla

F. Albino,[1] V. Pinel[1] and F. Sigmundsson[2]

[1] *Laboratoire de Géophysique Interne et Tectonophysique, CNRS, IRD, Université de Savoie, Campus Scientifique,* 73376 *Le Bourget du Lac Cedex, France. E-mail: Fabien.Albino@univ-savoie.fr*

[2] *Nordic Volcanological Center, Institute of Earth Sciences, Askja, University of Iceland Sturluga* 7, IS-101 *Reykjavik, Iceland*

Accepted 2010 March 15. Received 2010 January 26; in original form 2009 January 27

SUMMARY

We investigate how surface load variations around volcanoes act on shallow magma chambers. Numerical calculations are carried out in axisymmetric geometry for an elliptical chamber embedded in an elastic medium. Magma compressibility is taken into account. For variable chamber shape, size and depth, we quantify how unloading events induce magmatic pressure change as well as variation of the threshold pressure required for dyke initiation at the chamber wall. We evaluate the triggering effect of these surface events on onset of eruptions and find it depends strongly on the surface load location and the magma chamber shape. We apply this model to two active Icelandic subglacial volcanoes: Grímsvötn and Katla. The 2004 eruption of Grímsvötn was immediately preceded by a jökulhlaup, a glacial outburst flood of 0.5 km^3. We show that this event may have triggered the eruption only if the system was very close to failure conditions. Katla volcano is covered by the Mýrdalsjökull ice cap. An annual cycle, with up to 6 m change in snow thickness, occurs from winter to summer. As the seasonal snow load is reduced, a pressure decrease of the same order of magnitude as the load is induced within the magma storage zone. Our model predicts that, in the case of a spherical or horizontally elongated magma chamber, eruptions are more likely when the snow cover is smallest, which appears consistent with the fact that all the last nine major historical eruptions at Katla occurred during the summer period. The model predicts an increase in Coulomb stress around the caldera, up to 7 km from its centre, during unloading periods, enough to trigger earthquakes. Stress due to snow load variations, with focusing of it in weak zones near the caldera boundary, is considered a contributing factor to seasonal seismicity observed beneath Mýrdalsjökull.

Key words: Numerical solutions; Mechanics, theory, and modelling; Magma chamber processes; Volcano/climate interactions.

1 INTRODUCTION

Surface load redistribution events occur frequently in the vicinity of volcanoes. Some of these events, such as partial destruction of volcanic edifices (Siebert 1984; Pinel & Jaupart 2005) or flank destabilization (Tibaldi 2001; Manconi *et al.* 2009) are a direct consequence of eruptive product emplacement and stability, whereas other events such as water level changes (McGuire *et al.* 1997; Björnsson 2002; Carrivick *et al.* 2009) or ice loading variations (Sigvaldason *et al.* 1992; Jellinek *et al.* 2004) are due to external phenomena. Whatever their origin, such events can cause sudden perturbations in the stress field around a magmatic system, as well as changes in pressure within the stored magma. Such changes can be of the same order of magnitude as variations induced by seismic events (few kPa to few MPa), but occur over larger timescales (1 h to few years, according to the event). Previous work considering 2-D deformation of a cylindrical liquid-filled magma chamber (Pinel & Jaupart 2005) demonstrated that the sudden partial destruction of a volcanic edifice always induces a pressure decrease within the magma. It may either prevent or promote an eruption, depending on the magma chamber size and depth. Here we evaluate in detail how the shape of magma storage zone influences both magma pressure changes and stress field variations induced by surface load variations. Numerical calculations in an axisymmetrical half-space quantify these perturbations. The magma is modelled as a fluid embedded in a homogeneous, isotropic elastic medium. Both media are treated in the simplest way, but the coupling between magma pressure and host rock stress field is fully considered. The

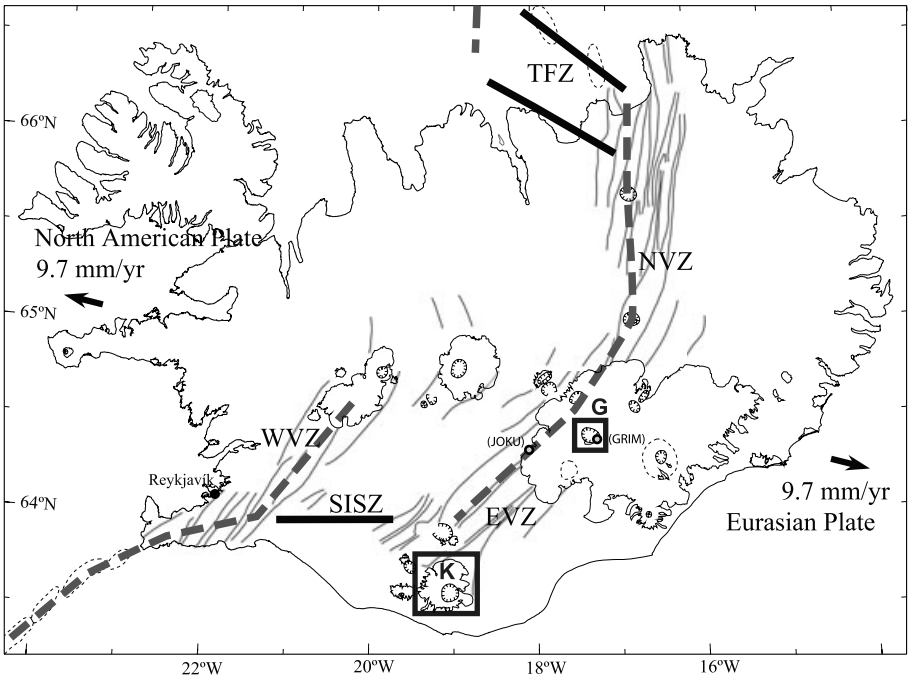

Figure 1. Map of Iceland showing the outline of fissure swarms along the central axis at the plate boundary (dashed grey line). Two transform zones, the South Iceland Seismic Zone (SISZ) and the Tjornes Fracture Zone (TFZ) are also indicated (black lines). Black boxes show the two study areas : G = Grímsvötn (64,42°N–17,33°W) under the Vatnajökull ice cap (8000 km^2) and K = Katla (63,63°N–19,05°W) under the Mýrdalsjökull ice cap (600 km^2). Two GPS stations GRIM and JOKU are located (modified from Sturkell *et al.* 2006).

influence of the depth, size and shape of a magma chamber, and also the distribution and extension of a surface load are systematically investigated.

The method developed is applied to two subglacial Icelandic volcanoes: Grímsvötn, where sudden glacial outburst floods (called jökulhlaups) originate, and Katla volcano, covered by an icecap of varying thickness (see Fig. 1 for location). Grímsvötn volcano has a caldera filled by a permanent subglacial lake where jökulhlaups occur typically at a frequency of 1–10 yr (Björnsson 2002). The eruption triggering effect of jökulhlaups at Grímsvötn was first proposed by Thorarinsson (1953) to explain an eruption in 1934. A jökulhlaup did also initiate before an eruption in November 2004 at Grímsvötn (Vogfjörd *et al.* 2005). However, in most cases, a jökulhlaup has not been followed by an eruptive event. In this study, we evaluate the ability of a jökulhlaup event to trigger an eruption. The other volcano studied here, Katla, is located beneath the Mýrdalsjökull ice cap whose load varies with time. Two types of load variations, with different temporal and spatial scales, have been described in a previous study (Pinel *et al.* 2007): an annual variation of the snow cover in the central part with an amplitude around 5 m, and a long-term decrease of the ice thickness, around 4 m yr^{-1}, at the periphery, due to the climate warming. A seasonality in seismic activity, with more events during the second half of the year, has also been demonstrated by Einarsson & Brandsdóttir (2000). Several cases of earthquake seasonality and ice cap/water loading have been studied previously (Heki 2003; Saar & Manga 2003; Bollinguer *et al.* 2007). However, none of these studies takes into account the presence of a magma chamber. Here we estimate the Coulomb stress change induced by the combined effect of surface load perturbation and consequent magma pressure re-equilibration, to evaluate seismicity rate variations. We consider the influence of the magma chamber shape, as well as the compressibility of the magma. At Katla, not only is there a relationship between ice load variations and seismicity, but also the onset of eruptions suggests a seasonal pattern; all nine large Katla eruptions since 1580 occurred in the period from May to November (Larsen 2000) when the ice load is reduced. In other areas, relationship between ice cap retreat and volcanic activity has been evaluated considering unloading effects on either the deep melt generation zone (Jull & McKenzie 1996; Pagli & Sigmundsson 2008), or the shallow magma storage zone (Gudmundsson 1986; Sigvaldason *et al.* 1992; Jellinek *et al.* 2004). Here we detail the effects of ice retreat on shallow magma chambers, considering the role of their variable depth, size and shape.

2 MODEL DESCRIPTION

2.1 General description, numerical method and main limitations

Host rock is treated as a homogeneous elastic medium characterized by its Young's modulus E, Poisson's ratio ν and tensile strength T_s. Based on the principle of superposition, we calculate stresses and displacement perturbations relative to a reference state which is considered to be lithostatic ($\sigma_{rr} = \sigma_{\theta\theta} = \sigma_{zz}$) (McGarr 1988). The sign convention used is such that tensile (compressive) stress is negative (positive). Magma modelled within the crust has a bulk modulus K and initial density equal to that of the crust (the magma chamber being at a level of neutral buoyancy). We model the magma as an inviscid liquid, considering that, given viscosity of magma ranging from 10 to 10^{10} Pa s (Spera 2000), the time delay required to reach a static equilibrium can be neglected for the load variations studied in this paper. No deviatoric stress is considered within the modelled magma chamber (Pinel & Jaupart 2003, 2005). Magma overpressure is therefore imposed by stress conditions applied to the

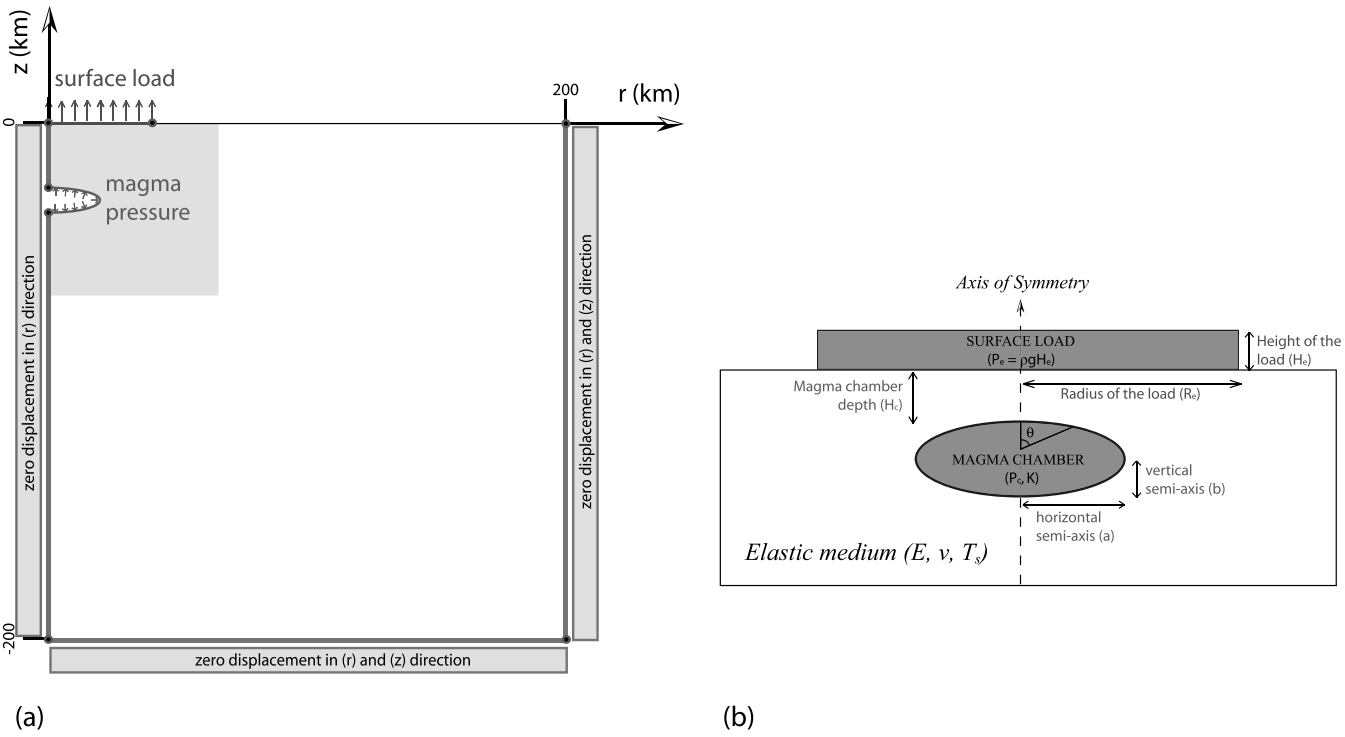

Figure 2. (a) Schematic view of the numerical model (a 200 × 200 km box in axisymmetrical geometry). Boundary conditions are the following: zero radial displacement on the axis of symmetry ($r = 0$), zero displacement at the edges of the box at $r = 200$ km and $z = -200$ km, a magma pressure P_c applied on the chamber wall, a normal stress P_e (negative for unloading) applied on a given area of the upper surface ($z = 0$), which otherwise is characterized by stress-free conditions. (b) Zoom of the zone of interest (grey area): magma chamber and surface load variation, showing all variable parameters.

solid at the chamber boundary, with a uniform normal stress, P_c, and no tangential stress. The so-called magma pressure, P_c, (subscript c for chamber) is actually an overpressure compared to the lithostatic state of reference. In the following, for a matter of simplicity, we will always use the term 'pressure' for the overpressure compared to the lithostatic state.

We use a 'Finite Element Method' (FEM) in axisymmetrical geometry considering the magma chamber as an elliptical volume. Load variation is modelled by a normal stress, negative value in the case of unloading, applied to a given area of the upper free surface. The following parameters are varied: (i) the chamber depth, H_c, measured from the chamber roof, (ii) the chamber size V_c, (iii) the chamber ellipticity ($\frac{a}{b}$), (iv) the load size (R_e) and (v) the load amplitude ($P_e = \rho g H_e$) (Fig. 2). Model dimensions are 200 × 200 km, with nearly 100 000 triangular elements. The relatively large model size compared to actual volcano size minimizes the influence of boundary conditions (zero displacement at infinity) applied at the edge of the model. Numerical results were validated by comparison with various existing analytical solutions (Mogi 1958; Fialko *et al.* 2001; Tsuchida *et al.* 1982).

The model presented here has some limitations due to the simplifying assumptions used. The medium is purely elastic, so viscoelastic behaviour is not taken into account. This is a limitation, but only for surface load variations occurring over a long period, such as sustained ice retreat (Jellinek *et al.* 2004; Pagli & Sigmundsson 2008). In the elastic solid, we consider only constant material properties, corresponding to an isotropic and homogeneous medium. In nature, there are heterogeneities in lithology and crustal structure which affect the magma path to the surface. For the magma inside a magma chamber, following Pinel & Jaupart (2005), we consider it as a homogeneous inviscid fluid with a constant internal overpressure and a given bulk modulus. We neglect viscosity and density change as well as processes related to gas accumulation and magma crystallization. These magma properties play an important role in eruption behaviour, but are not considered important for the load changes studied here. We thus assume that the amount of crystallization remains too small to describe the magma as a elastic solid softer than the encasing medium, as proposed by Manconi *et al.* (2009). Even though we make these simplifying assumption for the fluid phase, our model gives a good estimate of the magma pressure change inside the chamber induced by surface load perturbation, taking into account the compressibility of magma through its bulk modulus K.

2.2 Pressure variation within the magma chamber

Any given stress field change around a volcanic system results in magma pressure variation ΔP_c within the chamber. Following Pinel & Jaupart (2005), we calculate this pressure change using the superposition principle, estimating the volume change of the chamber for two distinct cases : (1) a chamber with an internal pressure change and no surface load change (ΔV_1); (2) a chamber with zero pressure change inside and a surface load change (ΔV_2). For each case, volume change is calculated numerically by integration of the normal displacement for each point of the mesh. The total volume change of the chamber, $\Delta V_c = \Delta V_1 + \Delta V_2$, is directly related to ΔP_c through the equation of state for the magma. In the incompressible case, the chamber volume is constant and $\Delta V_c = 0$. In the compressible case, the chamber volume change is related to the magma pressure change through the following relation:

$$\Delta V_c = -\frac{\Delta P_c V_c}{K} \quad (1)$$

with K being the magma bulk modulus (compressibility equals $\frac{1}{K}$). For magma with no exsolved gas, the bulk modulus K is estimated to be 10–40 GPa (Tait *et al.* 1989), with the smaller values for the more compressible magmas. However, if magma has exsolved gas, the compressibility may be much higher with values for K around 0.1–1 GPa (Huppert & Woods 2002).

2.3 Variation of the threshold pressure needed for dyke initiation

Before propagating towards the surface, dykes are initiated at the magma chamber wall by brittle failure of the crust. Rupture in mode I (tensile failure) is often used in studies of dyke propagation (Rubin 1993, 1995). Here we study the conditions required to cause such failure, focusing on tensile failure mechanism. Following Pinel & Jaupart (2003), we consider the deviatoric component, R, of the minimum compressive stress:

$$R = \sigma_3 - \frac{\sigma_1 + \sigma_2 + \sigma_3}{3} = \frac{2\sigma_3 - \sigma_1 - \sigma_2}{3}, \quad (2)$$

where $\sigma_1, \sigma_2, \sigma_3$ are the three principal stress components. Failure occurs when R, calculated at the chamber wall, compensates the tensile strength of the host rocks : $R = -T_s$. With this failure criteria, we determine the value of σ_1 corresponding to the minimum overpressure required inside the magma chamber to cause tensile failure. This pressure is here called threshold pressure for rupture, P_r (subscript r standing for rupture). As an example, a pressurized spherical chamber in an infinite medium has $\sigma_2 = \sigma_3 = -\frac{1}{2}\sigma_1$. The failure criteria simplifies to $-\frac{1}{2}\sigma_1 = -T_s$ and the classic rupture criteria for a sphere in an infinite medium, $P_r = 2T_s$, is obtained (Tait *et al.* 1989). Any surface load variations will perturb the subsurface stress field and thus modify the rupture conditions by inducing a change ΔP_r of the threshold pressure required to initiate dykes. The sign of ΔP_r can be either negative or positive, so surface load perturbation can either enhance or prevent initiation of dykes. However, as we said before, the load variation also affects magma pressure. Therefore, an exact estimation of the potential effect of a surface load event on dyke initiation requires a comparison between the two pressure changes: magma pressure change ΔP_c and threshold pressure change ΔP_r (Fig. 3).

2.4 Influence of surface load changes on eruption likelihood

Before a surface load change, the chamber is characterized by an initial state with a given pressure $P_c(i)$ and a threshold pressure required to initiate a dyke $P_r(i)$. The initial pressure difference $\Delta P_I = P_r(i) - P_c(i)$ is an indicator of the state of the magmatic

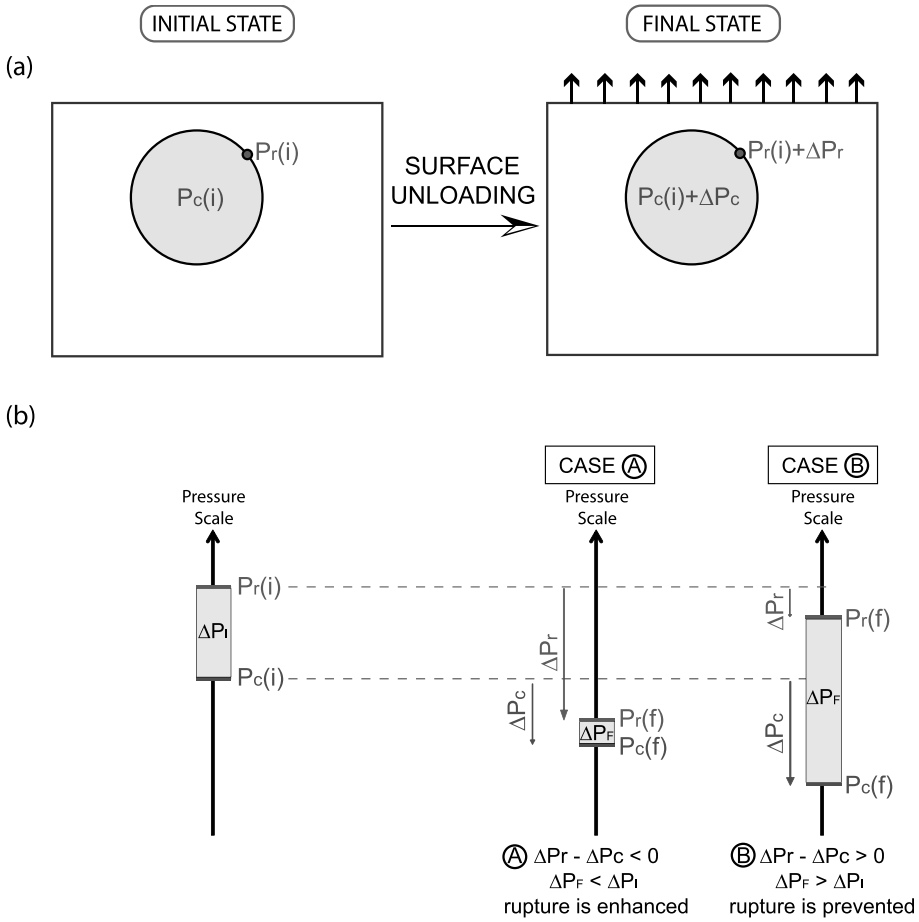

Figure 3. (a) Evolution of the magma pressure P_c and threshold pressure for failure P_r during an unloading event. (b) Evolution of the ability of the system to erupt. ΔP_I and ΔP_F represent the 'pressure gap' of the system necessary to initiate eruption, respectively before and after an unloading event. The final state depends on the initial state, the magma pressure change and the rupture threshold pressure change : $\Delta P_F = \Delta P_I + (\Delta P_r - \Delta P_c)$. When $\Delta P_F < \Delta P_I$ (case A), rupture is enhanced and may occur or not depending on the initial state. In the case $\Delta P_F > \Delta P_I$ (case B), no eruption will occur. All pressure values are perturbations compared to a lithostatic state of reference.

system. The smaller ΔP_I is, the closer to failure the system is. If a surface unloading event occurs, the pressure inside the chamber will decrease $P_\mathrm{c}(f) = P_\mathrm{c}(i) + \Delta P_\mathrm{c}$ (with ΔP_c always negative). The threshold pressure for rupture will also change : $P_\mathrm{r}(f) = P_\mathrm{r}(i) + \Delta P_\mathrm{r}$. The final pressure difference ΔP_F can be written as follows:

$$\begin{aligned}\Delta P_\mathrm{F} &= P_\mathrm{r}(f) - P_\mathrm{c}(f) \\ &= \Delta P_\mathrm{I} + (\Delta P_\mathrm{r} - \Delta P_\mathrm{c}).\end{aligned} \tag{3}$$

The failure of the magma chamber occurs and a dyke can be initiated when ΔP_F is equal to 0. The difference $(\Delta P_\mathrm{r} - \Delta P_\mathrm{c})$ provides the relative evolution of a magmatic system after an unloading event, characterizing the effect of this surface perturbation on dyke initiation at the chamber wall (Fig. 3b). Positive values indicate that the magma chamber moves away from failure conditions and dyke initiation is inhibited. Inversely, for negative values, the magma chamber approaches failure conditions and dyke initiation is favoured. Failure initiation at the chamber wall is a required condition for eruptions but does not necessary mean that an eruptive event will follow. An eruption occurs only if magma can propagate towards the surface which depends on the reservoir pressure as well as the stress field (Pinel & Jaupart 2004). However, here, we restrict our study to the effect on dyke initiation and consider that when dyke initiation is favoured, eruption likelihood increases.

2.5 Parameters investigated

The effect of a surface load change above a magma chamber was evaluated in a series of models, considering various parameters such as the chamber shape and the load distribution. Due to the axisymmetric geometry, effects of asymmetrical unloading events or dipping magma sources are beyond the scope of this study. Future 3-D models might take such parameters into consideration. For the surface load variation, we considered two classes of load change: a central load (a cylinder with a 5 km radius) and a peripheral load (a 'toroid' shaped with a cylinder of 10 km radius and a 5 km internal hole). The magma chamber is an ellipsoid, with ellipticity ($\frac{a}{b}$), volume ($V_\mathrm{c} = \frac{4}{3}\pi a^2 b$) and top depth ($H_\mathrm{c}$). We explored a likely depth range for shallow chambers in Icelandic volcanoes, from 2 to 7 km beneath the surface (Sigmundsson 2006). Chamber volumes are less well constrained, and we investigated a wide range from 0.5 to 50 km^3. Models have been calculated for chamber depths (H_c) of 1, 3 and 5 km, and for chamber volumes (V_c) of 0.5, 10 and 50 km^3. The chamber volume affects only the amplitude of the pressure difference $(\Delta P_\mathrm{r} - \Delta P_\mathrm{c})$, with larger values in the case of smaller chamber volumes, but has otherwise no significant effect on this difference as a function of chamber depth or ellipticity. Therefore, we only present the results for the intermediate volume $V_\mathrm{c} = 10\,\mathrm{km}^3$.

3 RESULTS

Results for the failure pressure change ΔP_r, the chamber pressure change ΔP_c and the difference between these two terms are shown in Figs 4 and 5, respectively, for the central and the peripheral model. Both confirm that a surface unloading event always induces a pressure decrease within the chamber, $\Delta P_\mathrm{c} < 0$. The failure pressure for a given state, P_r, is a function of the host rock tensile strength T_s. In the case of small amplitude surface load variations (less than 10 MPa), rupture at the chamber walls occurs at the same location before and after the unloading event and the resulting failure pressure variation ΔP_r does not depend on the value of T_s.

For a central load removal with lateral extension comparable to the chamber size, the magma pressure change (ΔP_c) gently increases with chamber ellipticity and is maximum for a horizontally elongated magma chamber (oblate) (Fig. 4b). Moreover, the magma pressure change is also controlled by the chamber depth, with high pressure drop for shallow chambers. The maximum amplitude is of the same order as the loading event. This pressure change decreases with more compressible magmas. The threshold pressure change, (ΔP_r), is slightly positive (less than $\frac{1}{4}$ of the load removed) for prolate ellipsoids, whereas it is negative, reaching larger values than the unloading event, for spherical and oblate ellipsoids (Fig. 4a). The amplitude of the surface unloading is important for shallow prolate and spherical chambers. The pressure change difference, $\Delta P_\mathrm{r} - \Delta P_\mathrm{c}$ (Fig. 4c), shows that a central unloading event inhibits rupture initiation for a prolate chamber (positive values) and promotes the rupture for a spherical and an oblate chamber (negative values). The enhancement of eruption likelihood is maximum for a spherical magma chamber situated at intermediate depth ($H_\mathrm{c} = 3$ km), and decreases with increasing chamber ellipticity. In the case of prolate chambers, the tendency to inhibit an eruption is more important for shallow chambers. Increasing compressibility of magma inside the chamber increases the 'enhancement effect' for spherical and oblate chambers, and reduces the 'inhibition effect' for prolate chambers.

For peripheral unloading, both pressure changes are smaller in amplitude than in the case of a central unloading event, with values always smaller than the surface load removed (Fig. 5). The maximum magma pressure change, ΔP_c, reaches only 40 per cent of the load removed and the amplitude of the difference, $\Delta P_\mathrm{r} - \Delta P_\mathrm{c}$, is always less than half of the load removed. Magma pressure changes strongly depend on the chamber shape as well as on its depth. As expected, for deep chambers ($H_\mathrm{c} = 5$ km) the results are similar to results for a central unloading event. Eruption is favoured for spherical and oblate chambers whereas it is inhibited for prolate chambers. For shallow chambers, magma pressure change ΔP_c is maximum for prolate ellipsoids, but tends to zero for oblate ellipsoids. Threshold pressure changes ΔP_r are negative for prolate shapes and positive for oblate shapes. In this case, an unloading event prevents rupture initiation, except for a prolate ellipsoid chamber filled with compressible magma. For an intermediate depth, magma pressure change ΔP_c is maximum for the spherical shape and the effect on eruption likelihood strongly depends on the amplitude of the load as well as the magma compressibility (Fig. 5c).

4 APPLICATION TO ICELANDIC SUBGLACIAL VOLCANOES

4.1 Lake discharge at Grímsvötn

4.1.1 The 2004 eruption

Grímsvötn volcano, located beneath the Vatnajökull ice cap (Fig. 1), is one of the most active volcanoes of Iceland, with about 70 eruptions in the last millennium (Thordarson & Larsen 2007). The volcano has a composite caldera of 8 km diameter, with a permanent subglacial lake (Fig. 6) (Björnsson & Einarsson 1990). This lake is formed by ice melting in response to the intense heat flux from geothermal and intermittent volcanic activity. The lake level increases to a threshold value above which lake discharge occurs. Such events, called jökulhlaup in Icelandic, are frequent in Iceland at intervals of 1–10 yr. They are sometimes associated

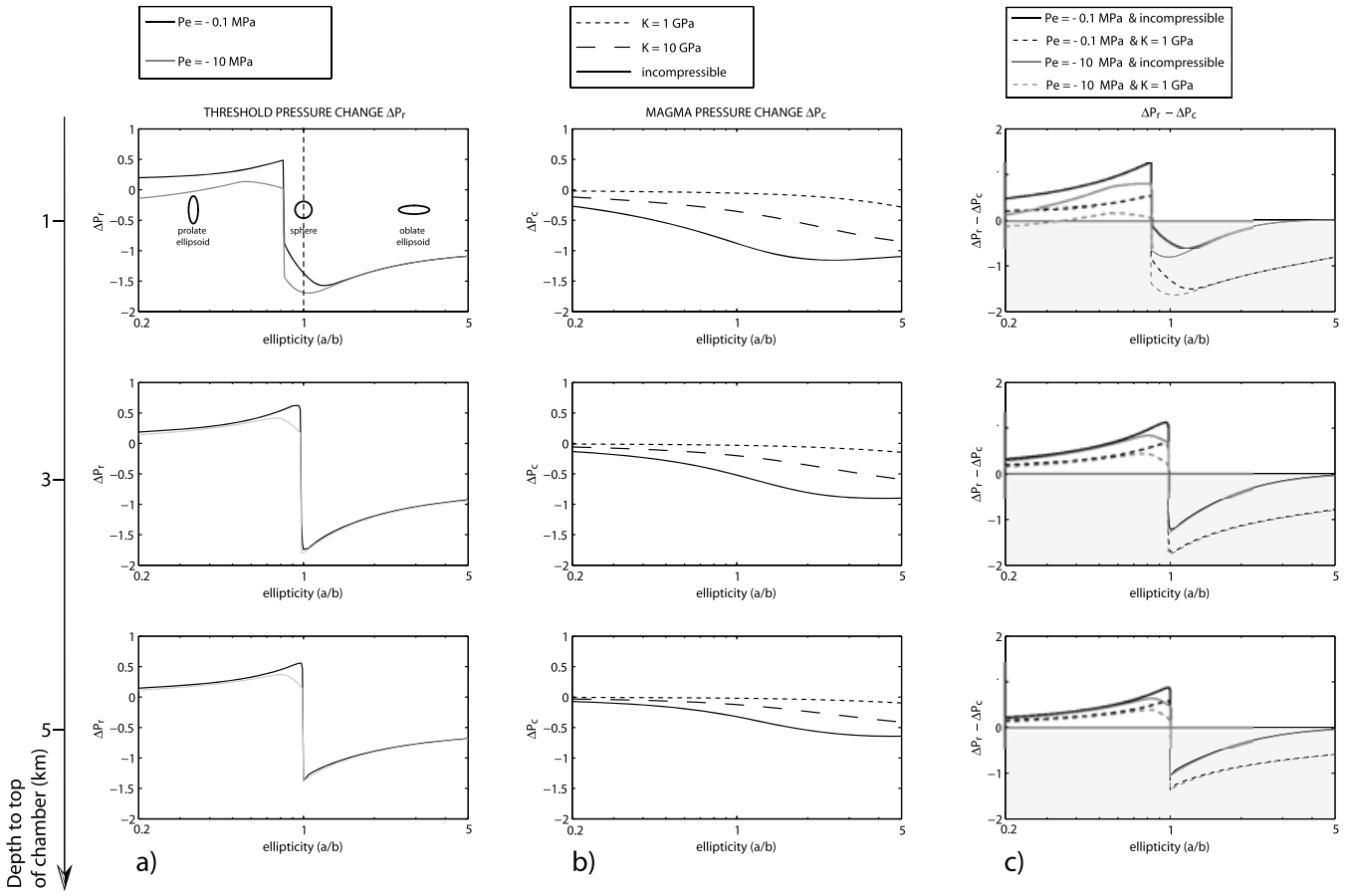

Figure 4. Evolution of pressure and rupture conditions for a magmatic system after a central unloading event. The load removed is a cylinder with 5 km radius. The magma chamber has a constant volume $V_c = 10\,km^3$. Calculations for three different chamber depths ($H_c = 1$, 3 and 5 km) are shown. All the pressure are normalized by the amplitude of the load removed. Results are obtained with $\nu = 0.25$, $E = 30$ GPa and $T_s = 20$ MPa. (a) The threshold pressure change ΔP_r as a function of the chamber ellipticity. The normalized pressure change depends slightly on the amplitude of the removed load, P_e. Results are shown for P_e equal to 0.1 and 10 MPa. (b) The magma pressure change within the chamber ΔP_c as a function of the chamber ellipticity. This change is highly dependent on the magma compressibility. Curves show values for K equal to 1 and 10 GPa as well as for the incompressible case. (c) $\Delta P_r - \Delta P_c$. The sign of this term indicates whether the magmatic system moves closer to or away from rupture conditions. Negative values (shaded area) mean that the unloading event promotes dyke initiation and thus the beginning of an eruption.

with eruptions as in 1934, 1938, 1983 and 2004 (Gudmundsson & Björnsson 1991; Björnsson 2002). An eruption, with high heat transfer, induces large ice melting which may be sufficient to initiate lake discharge if the lake level is close to a critical state. However, it has also been proposed that jökulhlaups and the associated pressure release can trigger volcanic eruptions, as in 1934 and more recently in 2004 (Thorarinsson 1974; Sigmundsson & Gudmundsson 2004).

The 2004 eruption started November 1 around 22 h GMT at the southwest caldera rim of Grímsvötn volcano. Increasing seismicity had been recorded by the Icelandic Meteorological Office's (IMO) monitoring system since the middle of 2003 (Vogfjörd *et al.* 2005) and continuous uplift of the surface had been measured by GPS at the GRIM station (located at 3 km from the caldera centre), since a previous eruption in 1998 (Fig. 7) (Sturkell *et al.* 2003, 2006). From geodetic, seismic and electric data, the chronology of the events for a few days before the eruption is well established (Vogfjörd *et al.* 2005). On October 28, episodes of harmonic tremor were recorded at seismic station KAL, situated 50 km south of Grímsvötn, indicating increased water flow under the Vatnajökull icecap covering Grímsvötn. The following day, electrical conductivity measurements in the Skeidará river, operated by the Icelandic Hydrological Service, revealed an increase of geothermal melt water and confirmed the beginning of a jökulhlaup. On October 30, icequakes were also detected in association with the jökulhlaup. The chronology of events shows the jökulhlaup began 3 days before the eruption. The discharge of Grímsvötn lake may therefore have triggered the eruption. Total lake discharge was estimated around $0.5\,km^3$ (Icelandic Hydrological Service), with a lake area evaluated around 10–11 km^2 (Berthier *et al.* 2006). *In situ* measurements at the subglacial lake with water-level gauges show that only 30 per cent of the total lake discharge occurred before the eruption, corresponding to a 15 m drop in lake level (H. Björnsson & F. Pálsson, personal communication, Oddsson 2007), equivalent to a pressure release at the caldera surface of 0.15 MPa. The geometry and the depth of a magma chamber under the Grímsvötn caldera are difficult to constrain. A seismic tomography survey (Alfaro *et al.* 2007) suggests a low velocity body under Grímsvötn, which can be interpreted as a magma chamber. A sill shaped geometry is suggested (2–2.5 km horizontal major axis and 0.5 km vertical minor axis) with a volume around $10\,km^3$ and top about 2.5 km under the caldera surface. This depth is consistent with the value of about 3 km (centre depth) estimated from deformation studies (Sturkell *et al.* 2003).

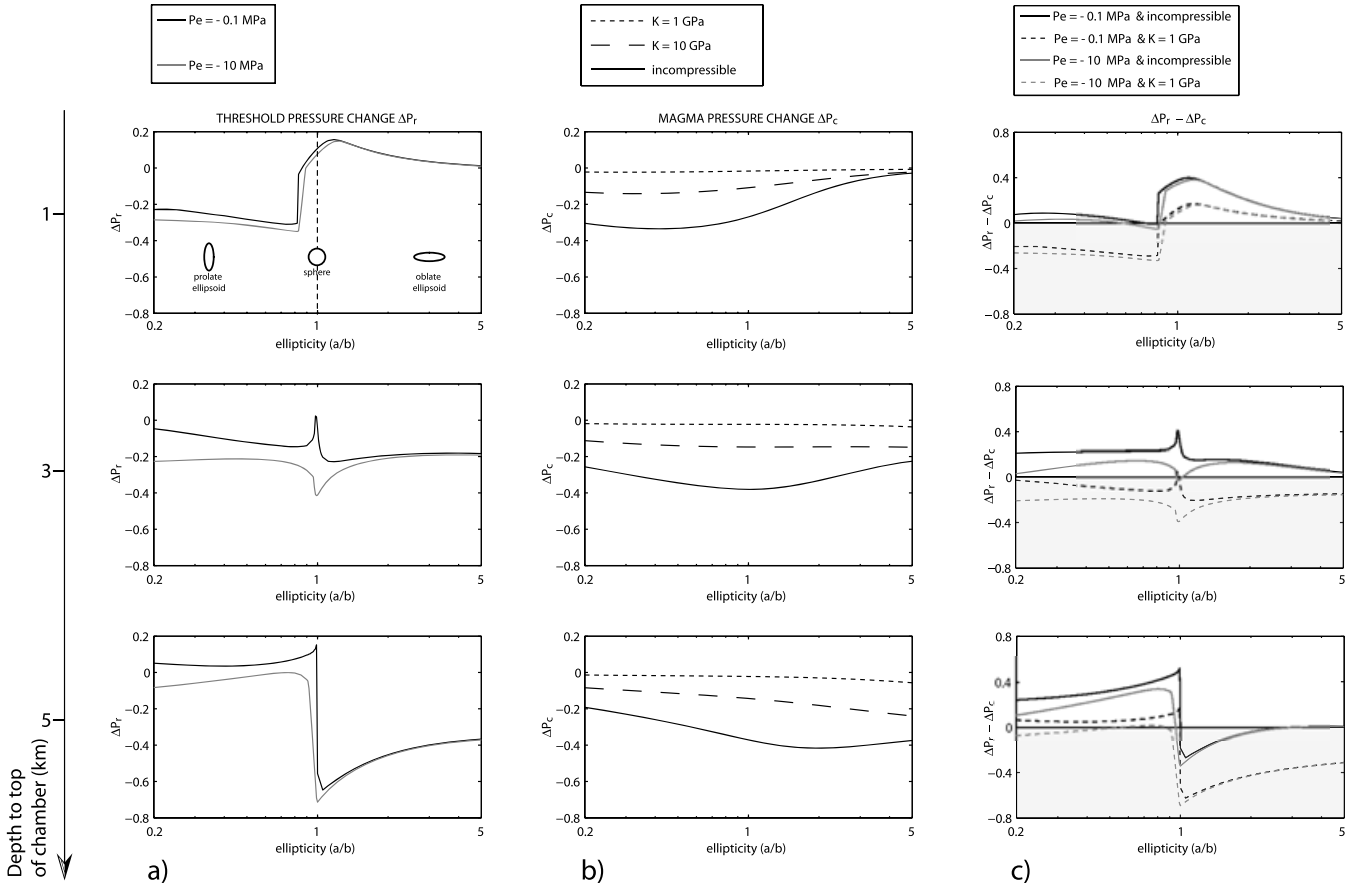

Figure 5. Evolution of pressure and rupture conditions for a magmatic system after a peripheral unloading event. Panels are the same as in Fig. 4, except the load removed has a toroid shaped with a 5 km internal radius and a 10 km external radius.

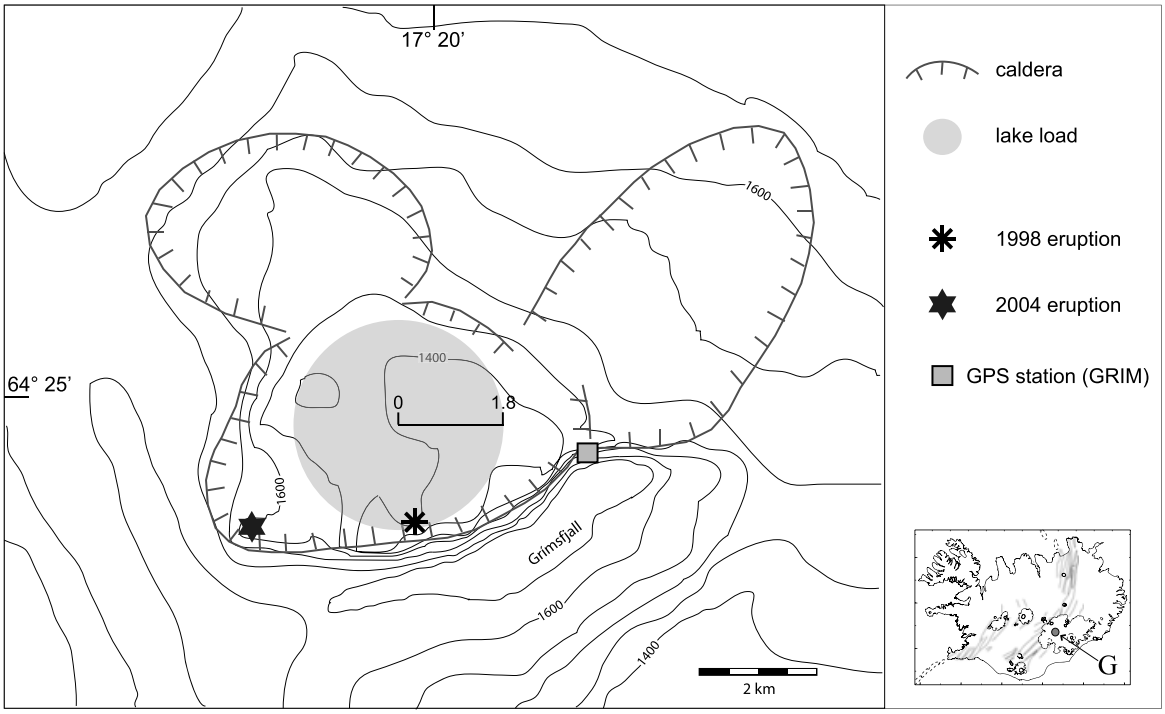

Figure 6. Grímsvötn ice surface map and caldera rim (modified from Gudmundsson & Björnsson 1991). Also shown are the 1998 and 2004 eruption sites, the disk load used to model the lake discharge in 2004 and GRIM GPS station. Inset map shows the location of Grímsvötn (G) within Iceland.

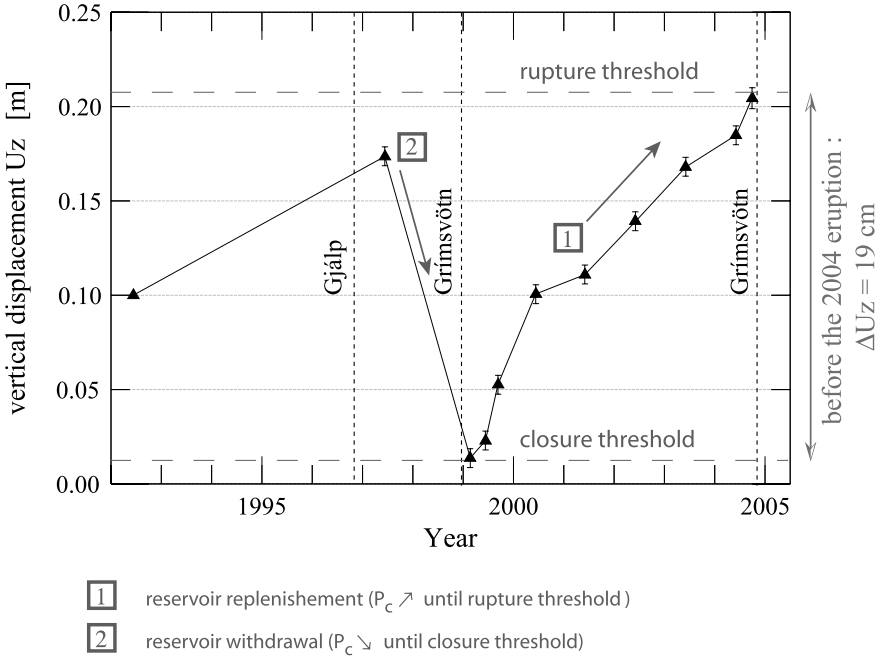

Figure 7. Interpretation of the vertical displacement recorded at the Grímsvötn GPS station (GRIM, located 3 km from the caldera centre) relative to a reference point at the Jökulheimar GPS station (JOKU, located 100 km west from the caldera centre) for the 1992–2005 period. Vertical uncertainty is ±4 mm. Modified from Sturkell *et al.* (2003).

4.1.2 Modelling of the 2004 jökulhlaup effect

We modelled the influence on eruption likelihood of the lake discharge which occurred prior to the eruption. Model values and results obtained are listed, respectively, in Tables 1 and 2. As the geometry of the magma chamber is poorly known, we considered two shapes (with a similar volume): an oblate (calculation 1) and a sphere (calculation 2). All calculations are for Young's modulus, E, equal to 30 GPa, considered appropriate for Icelandic crust (Pinel *et al.* 2007).

The 0.15 MPa pressure release at the surface, due to the 2004 jökulhlaup prior to eruption onset, induces a decrease of the threshold pressure for failure ΔP_r of about 0.04 MPa for an oblate chamber (calculation 1) and more than 0.15 MPa for a spherical chamber (calculation 2). As explained in Chapter 2, we also consider the variation in pressure inside the magma chamber ΔP_c induced by the jökulhlaup. The difference, $\Delta P_r - \Delta P_c$, characterizes the evolution of eruption likelihood. Values are negative for both geometries considered (except for the incompressible case in calculation 1), and larger for chambers filled with more compressible magma (lower bulk modulus). The modelling shows that the 2004 jökulhlaup and the associated surface pressure release favoured dyke initiation at the chamber wall and may have triggered the eruption. However, the effect is small. The amplitude of the effect ($\Delta P_r - \Delta P_c$) is maximum and equivalent to the surface load removed (around 0.15 MPa), for a spherical chamber filled with compressible magma. For an oblate chamber, the triggering effect reaches only 0.01 MPa for $K = 10$ GPa, which corresponds to only 5 per cent of the surface pressure change.

Table 1. Numerical values used to model the effect of the 2004 jökulhlaup at Grímsvötn.

	Unit	Symbol	Calculation 1 oblate	Calculation 2 sphere
Magma reservoir				
Horizontal axis	km	a	2.5	1.5
Vertical axis	km	b	0.5	1.5
Depth	km	H_c	2.5	1.5
Volume	km^3	V_c	13.09	14.14
Load removed[a]				
Lake radius	km	R_e	1.8	1.8
Water level drop	m	H_e	15	15
Pressure change	MPa	P_e	0.15	0.15

[a]The extension of the subglacial lake and characteristics of the jökulhlaup in 2004 are estimated from Berthier *et al.* (2006) and personal communication (H. Björnsson F. Pálsson).

As magma compressibility is a key parameter, we attempted to use GPS measurements to constrain its value for the magma stored at the Grímsvötn volcano. A cumulative vertical uplift of 19 cm was recorded at GRIM station (3 km east of the caldera centre) between the end of the 1998 eruption and the fall of 2004 (Fig. 7). With our model, this uplift can be attributed to a pressure increase in a magma chamber of 5.5 and 23.75 MPa, respectively, for the oblate shape (calculation 1) and the spherical shape (calculation 2). These values of pressure variations can be used as an estimation of the pressure drop during the 2004 eruption if we assume the pressure in the magma chamber at the end of an eruption was the same in 1998 and 2004. The pressure drop, together with an estimate of the erupted volume, around 0.02 km^3 dry rock equivalent (DRE) (Oddsson 2007), allows an estimation of magma compressibility. Considering that the chamber volume change is equal to the erupted volume, the magma bulk modulus obtained has a value of 15 GPa for the oblate chamber and the magma has to be incompressible for the spherical chamber. With these values of K, the corresponding pressure difference, $\Delta P_r - \Delta P_c$, is 0.005 MPa in case of an oblate ellipsoid and 0.13 MPa in case of a spherical chamber. From these results we conclude that the ability of the 2004 jökulhlaup to trigger an eruption indicates that before the lake discharge the magma

Table 2. Results for pressure changes due to the 2004 jökulhlaup event, considering magma reservoir and load parameters given in Table 1.

	Symbol	Calculation 1 oblate (MPa)	Calculation 2 sphere (MPa)
BEFORE THE 2004 JÖKULHLAUP EVENT			
Magma pressure	P_c	5.50	23.75
Adjusted tensile strength to have $\Delta P_I = 0$	T_s	22.00	13.88
AFTER THE 2004 JÖKULHLAUP EVENT			
Failure pressure change	ΔP_r	−0.040	−0.168
Magma pressure change	ΔP_c		
$K = \infty$		−0.045	−0.034[a]
$K = 20$ GPa		−0.036	−0.019
$K = 15$ GPa		−0.035[a]	−0.017
$K = 10$ GPa		−0.030	−0.013
Final pressure difference	ΔP_F		
$K = \infty$		$\Delta P_I + 0.005$	$\Delta P_I - 0.134$[a]
$K = 20$ GPa		$\Delta P_I - 0.004$	$\Delta P_I - 0.149$
$K = 15$ GPa		$\Delta P_I - 0.005$[a]	$\Delta P_I - 0.151$
$K = 10$ GPa		$\Delta P_I - 0.010$	$\Delta P_I - 0.155$

Note: Calculations are for $E = 30$ GPa and $\nu = 0.25$. ΔP_I and ΔP_F are indicators of the failure state of the magma chamber, respectively, before and after the load removed (see Section 2.4).
[a]Correspond to the values obtained using the magma bulk modulus calculated for the 2004 event (from the pressure drop and volume of the eruptive products estimations).

chamber was already very close to rupture conditions, with more than 99.5 per cent of the pressure threshold recovered inside the magma chamber since a previous eruption.

4.1.3 A more general view on the ability of jökulhlaups to trigger eruptions?

A jökulhlaup in 1996 was associated with a 100 m lake level drop, 10 times the 2004 event. This did not trigger an eruption at Grímsvötn (Björnsson 2002). For this event, the initial state of stress is poorly constrained as there was only one survey of the GRIM GPS site in 1992, and an other one in 1997. We consider that the pressure P_c within the magma chamber at the end of the 1998 eruption was zero (note again that P_c represents the overpressure compared to the lithostatic state of reference). It corresponds to the condition for dyke closure if viscous and thermal effects are neglected. Such effects could have stopped the eruption at a larger magma pressure. From Fig. 7, we can then estimate the magma pressure P_c before the 1996 unloading event, to have been around 4.2 and 18.25 MPa, respectively, for the oblate and the spherical chamber models. In this case, the magma pressure in 1996 was not close to the rupture conditions. We have an estimation of ΔP_I around 1.3 and 5.5 MPa, respectively, for oblate and spherical chambers (indicating that less than 80 per cent of the pressure threshold was recovered). The maximum $\Delta P_r - \Delta P_c$ pressure change induced by the 1996 jökulhlaup is 10 times larger than for the 2004 event, about 0.05 MPa for the oblate chamber and about 1.3 MPa for spherical chamber. In all cases, this triggering effect remains too small, compared to ΔP_I, to cause failure of the chamber wall and induce an eruption. In conclusion, when the lake discharge occurred at Grímsvötn caldera in 1996, although the triggering effect was larger in amplitude, the magma chamber was initially too far from rupture conditions and no eruption was initiated. A surface unloading event, such as lake discharge, is able to trigger the eruption only when the system is already very close to failure. This is consistent with the fact that only some jökulhlaups at Grímsvötn have triggered an eruption.

4.1.4 Estimation of the tensile strength

Even though it is a key parameter for characterizing crustal failure, the rocks tensile strength remains poorly constrained. Estimates come, for example from experimental studies which had problems reproducing large confining pressure conditions (Touloukian *et al.* 1981). Here we show how interpretation of deformation data, together with a model, can provide complementary constraint on the tensile strength. As previously shown, the values of 5.5 and 23.75 MPa (respectively for the calculation 1 and 2) represent the magma pressure changes P_c before the 2004 eruption (Table 2). As the reservoir was close to rupture conditions, these magma pressure values were very close to the failure pressure P_r. This assumption can be used to estimate numerically the rock tensile strength T_s. We obtain, respectively, 22 and 13.9 MPa for the T_s value for the oblate and the spherical chamber model (Table 2). These estimates are consistent with some reported values for tensile strength (Touloukian *et al.* 1981), although somewhat higher than the range 1–10 MPa measured in Iceland (Haimson & Rummel 1982).

4.2 Icecap load variations at Katla

4.2.1 General context

Katla is a subglacial volcano located in South Iceland under the Mýrdalsjökull ice cap (Björnsson *et al.* 2000; Thordarson & Larsen 2007) (Fig. 1). It has a NW–SE elongated caldera (9 × 14 km) from which 20 explosive eruptions have occurred in historical times, the most recent in 1918 (Larsen 2000). Although the details of a magma storage zone at shallow depth are debated (Óladóttir *et al.* 2008), there is seismic as well as geodetic evidence for a magma chamber. A 2-D seismic undershooting survey has shown traveltime anomalies at shallow levels, interpreted as a 5 km wide magma chamber with a bottom at 3 km below the surface (Gudmundsson *et al.* 1994). Other studies have estimated the depth of the magma chamber at about 5 km depth from crustal deformation results interpreted with a point

Table 3. Numerical values used to model the effect of ice/snow load variations at Katla.

	Unit	Symbol	Value
Magma reservoir[a]			
Horizontal axis	km	a	2.5
Vertical axis	km	b	0.5
Depth	km	H_c	2.5
Volume	km^3	V_c	13.09
Seasonal unloading[b]			
Pressure change for radius R_e: $0 < R_e < 7$ km	MPa	P_e	−0.042
Pressure change for radius R_e: $7 < R_e < 9.5$ km	MPa	$\frac{1}{2} P_e$	−0.021
Long-term unloading[b]			
Pressure change for radius R_e: $7 < R_e < 17$	MPa	P_e	−0.035

[a]Size, shape and depth of the Katla reservoir are estimated from Gudmundsson *et al.* (1994).
[b]Characteristics of the ice/snow thickness variation are estimated from Pinel *et al.* (2007).

source model (Sturkell *et al.* 2006; Sturkell *et al.* 2008). Parameters used in our calculation for the geometry of Katla's chamber are listed in Table 3.

Aeroplane radar measurements of surface elevation at Mýrdalsjökull acquired since 1999 show an annual cycle in its central part, as well as gradual ice thinning at the periphery of the ice cap (Gudmundsson *et al.* 2007). Snow accumulates during winter and melts during summer, while gradual ice thinning occurs in response to warmer climate. Pinel *et al.* (2007) modelled the displacements due to these two surface load variations, in order to discriminate between magma movement and surface load contributions to measured displacements. The seasonal effect is here modelled by a uniform snow disc load centred on the caldera, with 7 km radius and thickness of 6.5 m, surrounded by a 2.5 km wide zone with 3.25 m thickness change. For long-term ice thinning, a toroid shaped ice load with an internal radius of 7 km and external radius of 17 km is used (Table 3, Fig. 8). Densities used to calculate pressure change induced by load variations are 650 and 900 kg m^{-3}, respectively, for the snow and the ice.

4.2.2 Possible modulation of the volcanic activity

The last nine major Katla eruptions with known calendar dates all began between May and November (Larsen 2000). A correlation between timing of eruptions and ice load thickness may be considered. We calculated the influence of seasonal snow melt on eruption likelihood. Results are shown in Table 4. The $\Delta P_r - \Delta P_c$ difference is negative for compressible magma, indicating that the seasonal unloading event enhances dyke initiation although the suggested effect is small, around 0.01 MPa. Our results thus confirm the possible effect of seasonal unloading events on the onset of eruptions at Katla, with a larger effect for more compressible magma. This seasonal load variation may however modulate the timing of eruptions only if the rate of pressure increase in the magmatic system

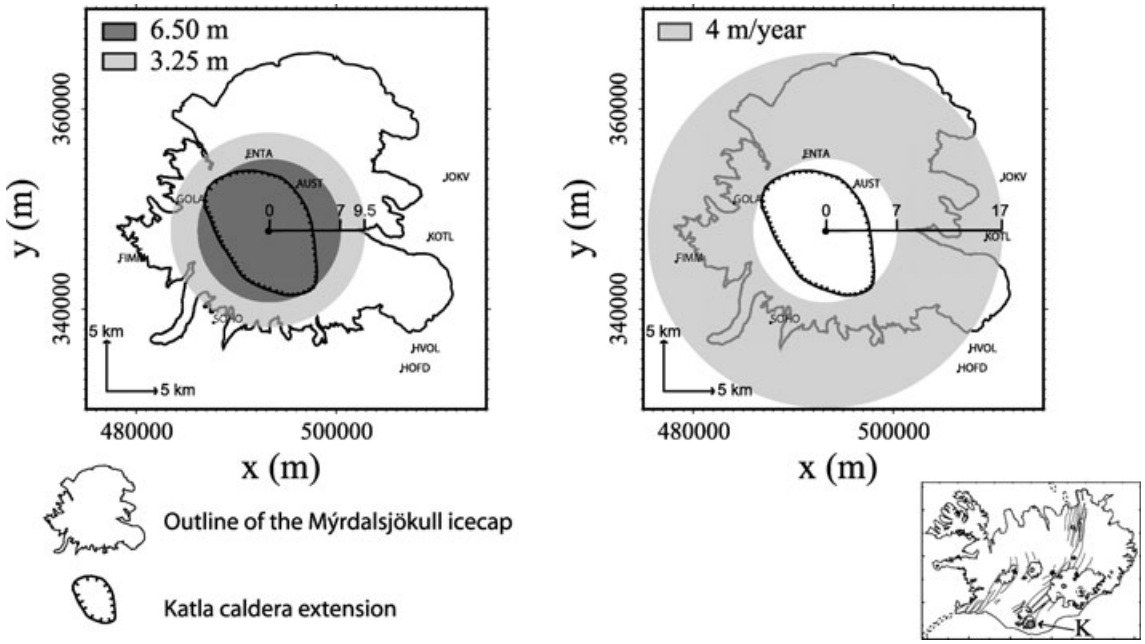

Figure 8. Model used to describe the two surface load variations at the Mýrdalsjökull icecap (modified from Pinel *et al.* 2007); left panel: central seasonal effect due to the snow cover variation between winter and summer period; right panel: peripheral long term effect due to the icecap retreat in relation with the warmer climate. Inset map shows the location of Katla volcano (K) within Iceland.

Table 4. Results for pressure changes due to the seasonal and long-term ice/snow loading event, considering a magma reservoir given in Table 3.

	Symbol	Value (MPa)
SEASONAL UNLOADING		
Failure pressure change	ΔP_r	-0.045
Magma pressure change	ΔP_c	
$K = \infty$		-0.046
$K = 20$ GPa		-0.037
$K = 10$ GPa		-0.031
Final pressure difference	ΔP_F	
$K = \infty$		$\Delta P_I + 0.001$
$K = 20$ GPa		$\Delta P_I - 0.008$
$K = 10$ GPa		$\Delta P_I - 0.014$
LONG-TERM UNLOADING		
Failure pressure change	ΔP_r	-0.0007
Magma pressure change	ΔP_c	
$K = \infty$		-0.0035
$K = 20$ GPa		-0.0029
$K = 10$ GPa		-0.0024
Final pressure difference	ΔP_F	
$K = \infty$		$\Delta P_I + 0.0028$
$K = 20$ GPa		$\Delta P_I + 0.0022$
$K = 10$ GPa		$\Delta P_I + 0.0017$

Note: Calculations are for $E = 30$ GPa and $\nu = 0.25$. ΔP_I and ΔP_F are indicators of the failure state of the magma chamber, respectively, before and after the load variations (see Section 2.4).

just before the eruption is small compared to the triggering effect. This implies a low magma inflow rate, with pressure increase on the order of 0.01 MPa yr^{-1} or less, inside the Katla chamber prior to eruption.

For long-term ice thinning, the yearly 0.035 MPa pressure release at the surface induces a decrease of 7×10^{-4} MPa in failure pressure and a decrease of 3.5×10^{-3} MPa in magma pressure. The difference, $\Delta P_r - \Delta P_c$, is always positive for all magma compressibilities. The long-term unloading inhibits dyke initiation at the chamber walls in the case of a laterally elongated chamber. The effect is smaller than the seasonal load, with an amplitude less than 0.003 MPa. However, for long-term unloading over decades, our model may not be appropriate as it does not consider viscoelastic relaxation in the lower crust and mantle.

4.2.3 Seasonal seismic activity

The Katla area has experienced persistent seismic activity since the beginning of seismic monitoring in the 1960s. The earthquake events are mostly located in two clusters, one inside the Katla caldera and another at Godabunga, a few kilometres west of the caldera rim. The seismicity has had a pronounced seasonal cycle for four decades, particularly in Godabunga, with more events occurring in the second half of the year (June to December). Einarsson & Brandsdóttir (2000) point out that a correlation exists between the seasonal seismic activity observed and the seasonal load change at the ice cap surface and/or the resulting change in crustal pore pressure beneath the icecap. They estimated the amplitude of the pore pressure effect to be larger than the load effect. Here, taking into account a magma chamber at depth, we investigate the total effect of the seasonal icecap load variation on the stress field and magma pressure, and the consequence for earthquake occurrence. The effects of the snow melt on pore pressure in the crust are not considered. For this study we use the Coulomb criterion, called CFF for Coulomb Failure Function. It provides a static stress measure of the proximity of a fault to failure, as done in many previous studies (Roman 2005; Árnadóttir *et al.* 2003). We evaluated the variation of this function or the Coulomb stress change, denoted ΔCFF. In our case, we considered the effect of surface unloading on particular fault planes, using the expression:

$$\Delta \mathrm{CFF} = \Delta\tau - \mu' \Delta\sigma_n, \tag{4}$$

where $\Delta\tau$ and $\Delta\sigma_n$ are, respectively, the variation of the shear and normal stress component resolved on a fault and μ' is the effective internal friction coefficient (King *et al.* 1994; King 2007). Positive Coulomb stress change signifies that earthquake occurrence is favoured. Coulomb stress changes are highly dependent on the geometry of the fault planes used in the calculation. In most cases, these planes are chosen based on geological information about the study area or on focal mechanism of triggered earthquakes (Walter *et al.* 2007; Roman 2005). However, this information is not available at Katla, so it is necessary to choose optimal planes associated with an initial stress field, often related to the tectonic context. Here, we consider the initial stress field as due to a pressurized magmatic system close to failure, and the Coulomb stress change is then calculated on the associated optimal planes. These planes are radial in the vicinity of the magma chamber wall.

Fig. 9 shows the results of the Coulomb stress change (ΔCFF) induced by seasonal load variations for three different magma chamber shapes (oblate, spherical and prolate ellipsoid). We also present a 'reference case' without any magma chamber. In that case, optimal planes are associated with an extensional tectonic regime. The main result is that the presence of a magma chamber strongly affects both the spatial distribution and the amplitude of the Coulomb stress change. Taking into account a magma chamber, ΔCFF maximum is not always located at the subsurface beneath the load but may be found at greater depth close to the chamber wall. Furthermore, the amplitude of the Coulomb stress change is always larger in the presence of a magma chamber. The amplitude of the effect increases with increasing magma compressibility. Maximum amplitude of ΔCFF is obtained for an oblate shaped chamber filled by compressible magma, with a value five times larger than the surface load variation and one order of magnitude larger than the 'reference case' without a magma chamber. In reality, the compressibility of magma lies between the two values used ($K = 1$ GPa and incompressible), with results shown on Fig. 9. The order of magnitude of Coulomb stress change is thus between 0.03 and 0.2 MPa, which is considered sufficient to trigger seismic events (Árnadóttir *et al.* 2003). However, the significance of this periodic Coulomb stress change (ΔCFF) depends on its amplitude relative to long-term stress change (Heki 2003). The annual load changes may modulate the occurrence of seismic activity only if the seasonal Coulomb stress change amplitude is of a similar order or higher than the long-term stress change. Another important factor is the spatial distribution of ΔCFF. Considering the presence of an oblate shaped magma chamber, maximum effect of the seasonal unloading is expected near the edge of the chamber at 2.5–5 km distance from the axis of symmetry. This effect may contribute to earthquake triggering in the main part of the Godabunga cluster, situated around 8–10 km west of Katla's centre. However, the highly clustered nature of the activity and the geographic position of this cluster with respect to the caldera led Soosalu *et al.* (2006) to suggest that the seismicity is the expression of an unstable cryptodome. In any case, the fact that the seasonal

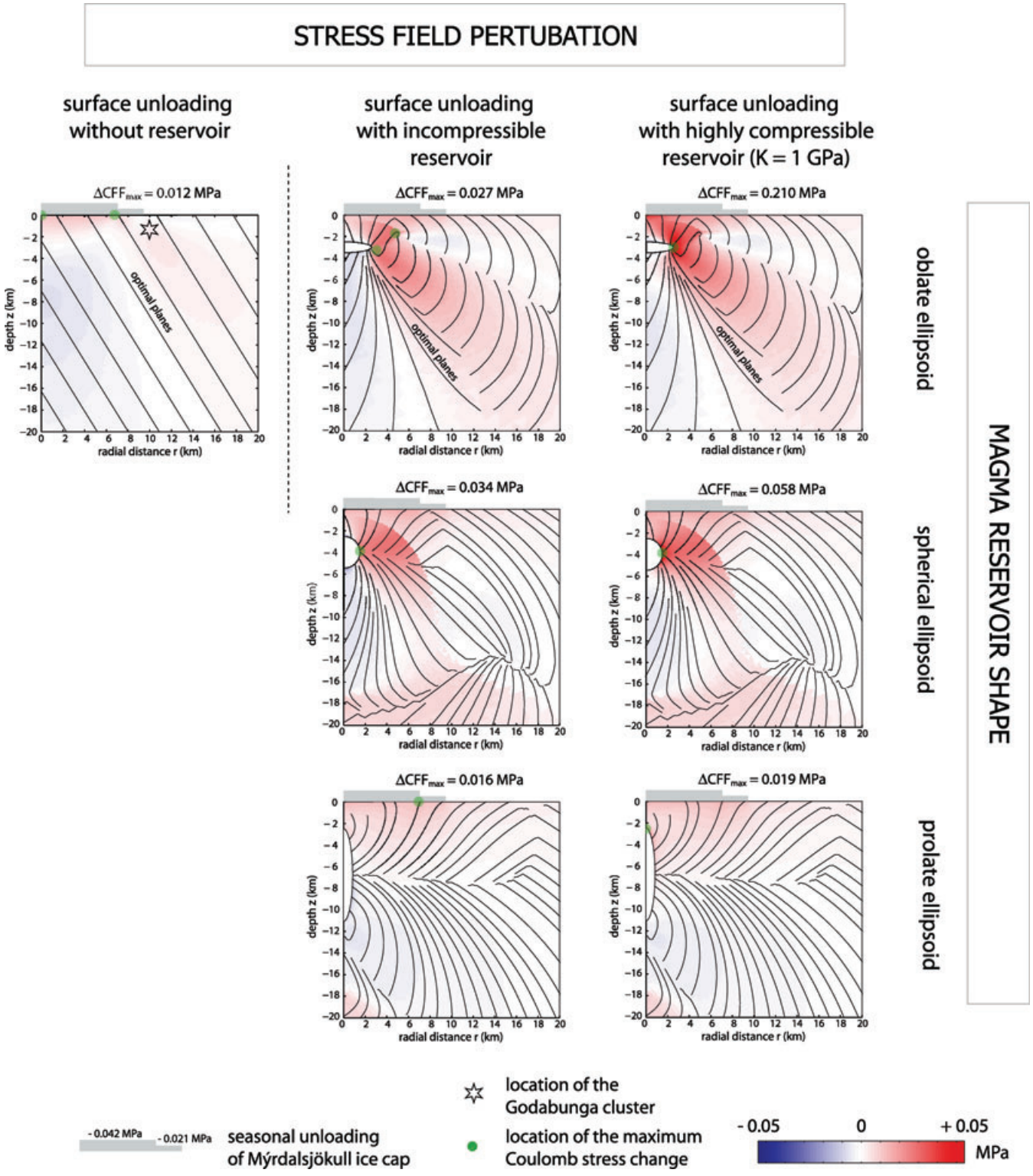

Figure 9. Coulomb stress change (ΔCFF) induced by the seasonal melt of snow at Katla volcano. ΔCFF is calculated on planes optimum for shear failure (shown with black lines) when the magma chamber is pressurized, with a surrounding lithostatic stress field. Parameters of the seasonal unloading as well as the chamber geometry are described in Table 3. Values of Young's modulus, Poisson's ratio and effective internal friction coefficient used are, respectively, 30 GPa, 0.25 and 0.5. Various reservoir shape (ellipticity equal to 5, 1 and 1/5) and magma compressibility are considered. In the top left panel, Coulomb stress change for a 'reference case' without magma chamber is calculated for an extensive regime associated with normal faulting. An indication of the location of the Godabunga cluster is shown (black star). For each model, location (green dots) and amplitude value of the maximum of Coulomb stress change is detailed.

seismicity is clustered at specific locations clearly indicates an heterogeneity either in fault distribution or in the initial stress field, neither of which are considered in our calculation. Around such heterogeneties, annual earthquake triggering can well be attributed to annual load changes. Our study also demonstrates the influence of magma chamber geometry on earthquake triggering. Seismicity rate response to the seasonal perturbation strongly depends on the shape and state of the magma reservoir. Katla's horizontally elongated magma chamber, indicated by the caldera structure itself as well as seismic studies (Gudmundsson *et al.* 1994), causes a larger triggering effect compared to other shapes. Moreover, the presence of the magma chamber at depth allows an amplification of the ice load effect, leading to ΔCFF changes higher than the surface pressure changes.

5 DISCUSSION AND CONCLUSION

Basaltic eruptions result from the propagation of magma through dykes, from the roof of a magma storage zone to the surface. The initiation of a dyke may be induced by a variation in the stress field within a crustal volume in the vicinity of a magma storage zone and/or by an increase of the magma pressure related to fluid dynamical changes (e.g. due to fresh magma replenishment, bubble gas accumulation and crystallization) (Tait *et al.* 1989). For example, seismic events induce stress field variations at short timescales in the crust and several studies have demonstrated interactions between large earthquakes and volcanic eruptions (Linde & Sacks 1998; Stein 1999; Feuillet *et al.* 2006; Walter *et al.* 2007). Three mechanisms have been proposed (Hill *et al.* 2002) to explain this relationship: (1) A static mode, that induces stress change only in the near field of the earthquake (within up to a few hundred km, depending on the earthquake magnitude); (2) a quasi-static mode, associated with the slow viscous relaxation of ductile lower crust and upper mantle; (3) a dynamic mode, due to the seismic wave propagation. This can influence a stress field at large distances, up to 1000 km or more. It can also modify the fluid pressure in magma and geothermal reservoirs by up to several kPa, by processes still being evaluated, such as rectified diffusion (Brodsky *et al.* 1998) or advective overpressure (Sahagian & Proussevitch 1992). For each mode, the stress variation depends strongly on the magnitude and the distance of the seismic event. For example, a M_w 8 earthquake occurring 100 km from a volcanic system induces a stress change of 0.1 and 3 MPa, respectively, in the static and dynamic states (Manga & Brodsky 2006). These amplitudes are relatively small compared to lithostatic pressures but not negligible when compared to the tensile strength of rocks. Such changes may be sufficient to activate a magmatic system already in a critical state. Moreover, the gas fraction in a magma mixture plays an important role in fluid pressure changes. Growth of bubbles mechanism can amplify magma pressure changes following external events, such as seismicity (Shimomura *et al.* 2006). However, earthquakes are not the only candidates for a triggering effect on magma storage zones. Global processes, external to volcanoes, may also have an effect. At short timescales, Earth tides with 0.001 MPa stress change in 12 h (Johnston & Mauk 1972) or daily variations in atmospheric pressure and temperature (Neuberg 2000) have also been proposed to explain volcanic modulation.

In this study, we demonstrate that unloading events occurring above volcanoes also have a triggering effect on eruption occurrence by modifying the ability of magma to leave the storage zone. We have focused on individualized shallow magma chambers, situated at few kilometres depth in the crust. These storage zones are often the result of magma accumulation at a neutral buoyancy level, where the density of magma is equivalent to the host rocks. We have also considered only eruptions fed by dykes which are initiated by tensile failure at the chamber walls. These eruptive conditions are mostly related to basaltic volcanoes, as in Iceland or Hawaii. In this volcanic context, our mechanical models provide new information on the possible interaction between surface load variations and magma storage. The main innovative aspect of our work is the exploration of the influence of different magma chamber shapes embedded in the crust, in an axisymmetric geometry. The consequences of this load redistribution on stress and pressure changes in the vicinity of the magma chamber are highly dependent on: (1) the shape of the magma chamber, (2) the compressibility of the magma and (3) the surface unloading amplitude and distribution. On the other hand, the magma chamber size has a small impact on results. For the Katla and Grímsvötn volcanoes, considering errors of ± 10 per cent for each semi-axis of the chamber, we obtained variations of a few kPa, for the pressure difference $\Delta P_r - \Delta P_c$ with higher values for smaller volumes. The triggering effect on a magmatic system induced by a surface load variation is typically of the same order of magnitude as the load removed. The maximum amplitude occurs for a spherical chamber filled with highly compressible magma.

Large flank collapses have a strong effect on magma storage zones, generating pressure changes exceeding 1 MPa (Manconi *et al.* 2009). Here, for the two Icelandic subglacial volcanoes studied, we demonstrated the potential triggering effect of smaller events such as lake water discharge and ice thickness variation on eruption likelihood. With a triggering amplitude of 1–10 kPa, these surface events have a larger effect than Earth tides and comparable to the static stress change induced by earthquakes. We confirm that jökulhlaups can trigger eruptions as observed at Grímsvötn in 2004, but only if an underlying magma chamber is close to failure conditions. Our study of the Katla magmatic system shows that the absence of historical eruptions during the winter period at Katla may relate to modulation of eruptive activity by the seasonal snow load variation. This implies low magma inflow rates prior to eruptions as otherwise the load effect would be insignificant relative to stresses induced by magma inflow. It follows that small deformation rates may be expected prior to eruptive events. We also emphasize the influence of surface load changes on the seismicity recorded around volcanoes. Study of Coulomb stress changes shows that seismicity changes induced by surface load variations are expected to be strongly dependent on the presence of a magma reservoir, its shape and the compressibility of the magma. Ideally, variations in recorded seismic activity such as at Katla may help constrain the shape and state of a magma reservoir.

ACKNOWLEDGMENTS

This study was supported by EU project VOLUME (Contract 18471). The authors are grateful to E. Sturkell, F. Pálsson and P. Einarsson for helpful discussions. The authors acknowledge insightful reviews by A. Manani and two anonymous referees. V.P. would like to dedicate this paper to Antoine Dubroca, who was born during the 2004 Grímsvötn eruption.

REFERENCES

Alfaro, R., Brandsdóttir B., Rowlands, D., White, R., &Gudmundsson, M.T., 2007. Structure of the Grimsvötn central volcano under the Vatnajökull icecap, Iceland, *Geophys. J. Int.,* **168,** 863–876.

Árnadóttir, T., Jonsson, S., Pedersen, R. & Gudmundsson, G., 2003. Coulomb stress changes in the South Iceland Seismic Zone due to two large earthquakes in June 2000, *Geophys. Res. Lett.,* **30,** 1205, doi:10.1029/2002GL016495.

Berthier, E., Björnsson, H., Pálsson, F., Feigl, K., Llubes, M. & Rémy, F., 2006. The level of the Grimsvötn subglacial lake, Vatnajökull, Iceland, monitored with SPOT5 images, *Earth planet. Sci. Lett.,* **243,** 293–302.

Björnsson, H., 2002. Subglacial lakes and jökulhlaups in Iceland, *Glob. Planet. Change,* **35,** 255–271.

Björnsson, H. & Einarsson, P., 1990. Volcanoes beneath Vatnajökull, Iceland: evidence from radio echo-sounding, earthquake and jökulhlaups, *Jökull,* **40,** 147–168.

Björnsson, H., Pálsson, F. & Gudmundsson, M.T., 2000. Surface and bedrock topography of the Mýrdalsjökull ice cap, Iceland, *Jökull,* **49,** 29–45.

Bollinguer, L., Perrier, F., Avouac, J.-P., Sapkota, S., Gautam, U. & Tiwari, D., 2007. Seasonal modulation of seismicity in the Himalaya of Nepal, *Geophys. Res. Lett.,* **34,** L08304.

Brodsky, E., Sturtevant, B. & Kanamori, H., 1998. Earthquakes, volcanoes, and rectified diffusion, *J. geophys. Res.,* **103,** 23 827–23 838.

Carrivick, J., Manville, V. & Cronin, S., 2009. A fluid dynamics approach to modelling the 18th March 2007 lahar at Mt. Ruapehu, New Zealand, *Bull. Volcanol.,* **71**(2), 153–169.

Einarsson, P. & Brandsdóttir, B., 2000. Earthquakes in the Mýrdalsjökull area, Iceland, 1978-1985: seasonal correlation and connection with volcanoes, *Jökull,* **49,** 59–73.

Feuillet, N., Cocco, M., Musumeci, C. & Nostro, C., 2006. Stress interaction between seismic and volcanic activity at Mt Etna, *Geophys. J. Int.,* **164,** 697–718.

Fialko, Y., Khazan, Y. & Simons, M., 2001. Deformation due to a pressurized horizontal circular crack in an elastic half-space, with applications to volcano geodesy, *Geophys. J. Int.,* **146,** 181–190.

Gudmundsson, A., 1986. Mechanical aspects of postglacial volcanism and tectonics of the of Reykjanes peninsula, Southwest Iceland, *J. geophys. Res.,* **91,** 12 711–12 721.

Gudmundsson, M.T. & Björnsson, H., 1991. Eruptions in Grimsvötn, Vatnajökull, Iceland, 1934–1991, *Jökull,* **41,** 21–44.

Gudmundsson, M.T., Högnadóttir, T., Kristinsson, A. & Gudbjörnsson, S., 2007. Geothermal activity in the subglacial Katla caldera, Iceland, 1999–2005, studied with radar altimetry, *Ann. Glaciol.,* **45,** 66–72.

Gudmundsson, O., Brandsdóttir, B., Menke, W. & Sigvaldason, E., 1994. The crustal magma chamber of the Katla volcano in south Iceland revealed by 2-D seismic undershooting, *Geophys. J. Int.,* **119,** 277–296.

Haimson, B. & Rummel, F., 1982. Hydrofracturing stress measurements in the Iceland research drilling project drill hole at Reydarfjordur, Iceland, *J. geophys. Res.,* **87,** 6631–6649.

Heki, K., 2003. Snow load and seasonal variation of earthquake occurence in Japan, *Earth planet. Sci. Lett.,* **207,** 159–164.

Hill, D., Pollitz, F. & Newhall, C., 2002. Earthquake-volcano interactions, *Phys. Today,* **55,** 41–47.

Huppert, H. & Woods, A., 2002. The role of volatiles in magma chamber dynamics, *Nature,* **420,** 493–495.

Jellinek, A., Manga, M. & Saar, M., 2004. Did melting glaciers cause volcanic eruptions in eastern California? Probing the mechanics of dike formation, *J. geophys. Res.,* **109,** B09206.

Johnston, M. & Mauk, F., 1972. Earth tides and the triggering of eruptions from Mount Stromboli, Italy, *Nature,* **239,** 266–267.

Jull, M. & McKenzie, D., 1996. The effect of deglaciation on mantle melting beneath Iceland, *J. geophys. Res.,* **101,** 21 815–21 828.

King, G., 2007. *Fault Interaction, Earthquake Stress Changes and the Evolution of Seismicity*, vol. 4, Elsevier, Gerald Schulbert edn.

King, G., Stein, R. & Lin, J., 1994. Static stress changes and the triggering of earthquakes, *Bull. seism. Soc. Am.,* **84,** 935–953.

Larsen, G., 2000. Holocene eruptions within the Katla volcanic system, south Iceland: characteristics and environmental impact, *Jökull,* **49,** 1–28.

Linde, A. & Sacks, I., 1998. Triggering of volcanic eruptions, *Nature,* **395**(6705), 888–890.

Manconi, A., Longpré, M.-A., Walter, T., Troll, V. & Hansteen, T., 2009. The effects of flank collapses on volcano plumbing systems, *Geology,* **37**(12), 1099–1102.

Manga, M. & Brodsky, E., 2006. Seismic triggering of eruptions in the far field: Volcanoes and geysers, *Ann. Rev. Earth planet. Sci.,* **34,** 263–291.

McGarr, A., 1988. On the state of lithospheric stress in the abscence of applied tectonic forces, *J. geophys. Res.,* **93,** 13 609–13 617.

McGuire, W., Howard, R., Firth, C., Solow, A., Pullen, A., Saunders, S., Stewart, I. & Vita-Finzi, C., 1997. Correlation between rate of sea level and frequency of explosive volcanism in the Mediterranean, *Nature,* **389,** 473–476.

Mogi, K., 1958. Relations between the eruptions of various volcanoes and the deformation of the ground surfaces around them, *Bull. Earthq. Res. Inst., Un. Tokyo,* **36,** 99–134.

Neuberg, J., 2000. External modulation of volcanic activity, *Geophys. J. Int.,* **142,** 232–240.

Oddsson, B., 2007. The Grímsvötn Eruption in 2004: dispersal and Total Mass of Tephra and Comparison with Plume Transport Models, *PhD thesis*, University of Iceland.

Óladóttir, B., Sigmarsson, O., Larsen, G. & Thordarson, T., 2008. Katla volcano, Iceland: magma composition, dynamics and eruption frequency as recorded by Holocene tephra layers, *Bull. Volcanol.,* **70**(4), 475–493.

Pagli, C. & Sigmundsson, F., 2008. Will present glacier retreat increase volcanic activity? Stress induced by recent glacier retreat and its effect on magmatism at the Vatnajökull ice cap, Iceland, *Geophys. Res. Lett.,* **35,** L09304.

Pinel, V. & Jaupart, C., 2003. Magma chamber behaviour beneath a volcanic edifice, *J. geophys. Res.,* **108,** 2072.

Pinel, V. & Jaupart, C., 2004. Likelihood of basaltic eruptions as a function of volatile content and volcanic edifice size, *J. Volcanol. Geotherm. Res.,* **137,** 201–217.

Pinel, V. & Jaupart, C., 2005. Some consequences of volcanic edifice destruction for eruption conditions, *J. Volcanol. Geotherm. Res.,* **145,** 68–80.

Pinel, V., Sigmundsson, F., Geirsson, H., Einarsson, P., Gudmundsson, M.T. & Högnadóttir, T., 2007. Discriminating volcano deformation due to magma movements and variable surface loads: application to katla subglacial volcano, iceland, *Geophys. J. Int.,* **169,** 325–338.

Roman, D., 2005. Numerical models of volcanotectonic earthquake triggering on non-ideally oriented faults, *Geophys. Res. Lett.,* **32,** L02304.

Rubin, A., 1993. Tensile fracture of rock at high confining pressure: implications for dyke propagation, *J. geophys. Res.,* **98**(B9), 15 919–15 935.

Rubin, A., 1995. Propagation of magma-filled cracks, *Ann. Rev. Earth planet. Sci.,* **23,** 287–336.

Saar, M. & Manga, M., 2003. Seismicity induced by seasonal groundwater recharge at Mt. Hood, Oregon, *Earth planet. Sci. Lett.,* **214,** 605–618.

Sahagian, D. & Proussevitch, A., 1992. Bubbles in volcanic systems, *Nature,* **359,** 485.

Shimomura, Y., Nishimura, T. & Sato, H., 2006. Bubble growth processes in magma surrounded by an elastic medium, *J. Volcanol. Geotherm. Res.,* **155,** 307–322.

Siebert, L., 1984. Large volcanic debris avalanches—characteristics of source areas, deposits, and associated eruptions, *J. Volcanol. Geotherm. Res.,* **22,** 163–197.

Sigmundsson, F., 2006. *Iceland Geodynamics, Crustal Deformation and Divergente Plate Tectonics*, Praxis Publishing—Springer-Verlag, Chichester.

Sigmundsson, F. & Gudmundsson, M.T., 2004. The Grimsvötn eruption, November 2004, *Jökull,* **54,** 139–142.

Sigvaldason, G., Annertz, K. & Nilsson, M., 1992. Effect of glacier loading/deloading on volcanism: postglacial volcanic production rate of the Dyngjufjiil area, central Iceland, *Bull. Volcanol.,* **54,** 385–392.

Soosalu, H., Jónsdóttir, K. & Einarsson, P., 2006. Seismicity crisis at the Katla volcano, Iceland-signs of a cryptodome?, *J. Volcanol. Geotherm. Res.,* **153,** 177–186.

Spera, F., 2000. *Encyclopedia of Volcanoes*, Physical properties of magma, Academia Press, New York.

Stein, R., 1999. The role of stress transfer in earthquake occurence, *Nature,* **402,** 605–609.

Sturkell, E., Einarsson, P., Sigmundsson, F., Hreinsdóttir, S. & Geirsson, H., 2003. Deformation of Grimsvötn volcano, Iceland: 1998 eruption and subsequent inflation, *Geophys. Res. Lett.,* **30,** 1182.

Sturkell, E. *et al.*, 2006. Volcano geodesy and magma dynamics in Iceland, *J. Volcanol. Geotherm. Res.,* **150,** 14–34.

Sturkell, E. *et al.*, 2008. Seismic and geodetic insights into magma accumulation at Katla subglacial volcano, Iceland: 1999 to 2005, *J. geophys. Res.,* **113,** B03212.

Tait, S., Jaupart, C. & Vergniolle, S., 1989. Pressure, gas content and eruption periodicity of a shallow, crystallising magma chamber, *Earth planet. Sci. Lett.,* **92,** 107–123.

Thorarinsson, S., 1953. Some new aspects of the Grímsvötn problem, *J. Glaciol.,* **2,** 267–276.

Thorarinsson, S. 1974. *The swift flowing rivers: the history of Grimsvötn jökulhlaups and eruptions.*, Menningarsjodur, Reykjavik.

Thordarson, T. & Larsen, G., 2007. Volcanism in Iceland in historical time: volcano types, eruption styles and eruptive history, *J. Geodyn.,* **43,** 118–152.

Tibaldi, A., 2001. Multiple sector collapses at Stromboli volcano, Italy: how they work, *Bull. Volcanol.,* **63,** 112–125.

Touloukian, Y.S., Judd, W.R. & Roy, R.F., 1981. *Physical Properties of Rocks and Minerals*, McGraw-Hill, New-York.

Tsuchida, E., Saito, Y., Nakahara, I. & Kodama, M., 1982. Stresses in a semi-infinite elastic body containing a prolate spheroidal cavity subjected to an axisymmetric pressure, *Jpn. Soc. Mech. Eng. Bull.,* **25**(204), 891–897.

Vogfjörd, K. *et al.*, 2005. Forecasting and Monitoring a Subglacial Eruption in Iceland, *EOS, Trans. Am. geophys. Un.,* **86**(26), 245–252.

Walter, T., Wang, R., Zimmer, M., Grosser, H., Lühr, B. & Ratdomopurbo, A., 2007. Volcanic activity influenced by tectonic earthquakes: Static and dynamic stress triggering at Mt. Merapi, *Geophys. Res. Lett.,* **34,** L05304.